Time-domain oversampled orthogonal signal-division multiplexing underwater acoustic communications

Jing Han,[1,a)] Yujie Wang,[1] Lingling Zhang,[1] and Geert Leus[2]
[1]*School of Marine Science and Technology, Northwestern Polytechnical University, Xi'an 710072, China*
[2]*Faculty of Electrical Engineering, Mathematics and Computer Science, Delft University of Technology, Delft 2826 CD, The Netherlands*

(Received 15 July 2018; revised 12 December 2018; accepted 16 December 2018; published online 22 January 2019)

Orthogonal signal-division multiplexing (OSDM) is a recently emerging modulation scheme which, compared to conventional orthogonal frequency-division multiplexing, can effectively lower the peak-to-average power ratio and introduce intra-vector frequency diversity. In this paper, a time-domain oversampled OSDM system for underwater acoustic (UWA) communications is designed, where each OSDM vector is equivalently transmitted over multiple virtual channels, and thus an enhanced frequency diversity gain can be achieved. Moreover, at the receiver, zero vectors and frequency-shifted Chu sequences are used for Doppler compensation and channel estimation, respectively, while low-complexity per-vector equalization is performed based on the composite channel matrix factorization. Finally, the performance of the proposed OSDM system is evaluated through both numerical simulations and a short-range field experiment, and its effectiveness over time-varying UWA channels is confirmed. © *2019 Acoustical Society of America.*
https://doi.org/10.1121/1.5087131

[JFL] Pages: 292–300

I. INTRODUCTION

Underwater acoustic (UWA) channels are considered as one of the most challenging communication media in use.[1] The low velocity of acoustic waves (nominally 1500 m/s) leads to a long multipath delay spread, which typically spans several tens of symbol intervals and thus causes severe inter-symbol interference (ISI).[2,3] To combat this effect and achieve high-rate transmissions, orthogonal frequency-division multiplexing (OFDM) and its frequency-domain equalization techniques have been widely investigated in recent UWA applications.[4]

Compared to conventional single-carrier modulation with adaptive time-domain equalization,[5,6] which is in general computationally intensive,[7] frequency-domain equalization for OFDM has low complexity. Specifically, OFDM can convert a frequency-selective channel into a set of parallel frequency-flat subchannels through the inverse discrete Fourier transform (IDFT) and discrete Fourier transform (DFT) processing at the transceiver. Each subchannel corresponds to a subcarrier of OFDM; therefore, simple one-tap equalization is enabled on each subcarrier to eliminate ISI.[8] However, it is well-known that OFDM systems suffer from a large peak-to-average power ratio (PAPR).[9,10] Moreover, since each data symbol is transmitted only over a single flat subchannel that may undergo fading, OFDM also suffers from a loss of multipath diversity.[4] As a countermeasure, OFDM usually resorts to channel coding, which, however, may significantly sacrifice bandwidth efficiency.

The newly emerging orthogonal signal-division multiplexing (OSDM) scheme is promising to address the above two problems inherent to OFDM systems. It was first proposed in Refs. 11 and 12, and shares a similar signal model with another scheme named vector OFDM proposed in Ref. 13. Specifically, OSDM provides a generalized modulation framework, which contains OFDM and single-carrier block transmission (SCBT) as two extreme cases.[14,15] It splits the data block into several vectors and performs component-wise IDFTs with a length reduced to the number of vectors, by which a lower PAPR can be achieved at the cost of bandwidth management flexibility.[14] Meanwhile, OSDM also enjoys intra-vector frequency diversity gain,[15] and thus can offer a superior performance compared to its OFDM counterpart over fading channels.

So far, there has been not much research on OSDM for UWA communications. The first attempt to establish an OSDM link over UWA channels was made in Ref. 16. It used multi-element reception, while assuming the channels to be static within a block. Preliminary results from a tank test suggested that OSDM can be a viable modulation scheme to achieve reliable UWA communications. A follow-up work in Ref. 17 explicitly modeled the channel doubly selective fading using a basis expansion model, by which a Doppler-resilient OSDM receiver was proposed to enhance the system robustness against the channel time variations. A more recent work in Ref. 14 further clarified that the Doppler distortion in OSDM can be modeled as inter-vector interference (IVI), which is analogous to inter-carrier interference in OFDM. Based on that, an iterative per-vector equalization scheme was designed to counteract the IVI-induced performance degradation. Moreover, space-frequency coded OSDM was also studied in Ref. 18 to exploit the transmit diversity gain. All these existing OSDM systems employ symbol-rate sampling at the receiver.

[a)]Electronic mail: hanj@nwpu.edu.cn

In this paper, we design a time-domain oversampled OSDM system over time-varying UWA channels. Our aim here is to further explore diversity gain to enable a more reliable transmission compared to standard symbol-rate sampling OSDM. Actually, time-domain oversampling has already been adopted in OFDM to introduce multipath diversity.[19,20] For OSDM systems, it can be used to increase the intra-vector frequency diversity and thus improve the system performance. The main contributions of this paper are summarized as follows.

- The signal model of time-domain oversampled OSDM is derived, from which it is shown that: (1) the time-domain oversampled OSDM vectors can be decoupled at the receiver over frequency-selective fading channels, and (2) each vector in time-domain oversampled OSDM is equivalently transmitted over multiple virtual channels, and thus diversity gain can be achieved.
- A time-domain oversampled OSDM receiver is also designed for time-varying UWA channels. It first performs Doppler compensation and channel estimation by using zero vectors and frequency-shifted Chu sequences, respectively. Then, per-vector oversampled equalization follows to obtain the OSDM symbol estimates. Here, the equalization algorithm is implemented based on matrix factorization of the composite channel matrix, which has approximately a linear complexity.

The remainder of this paper is organized as follows. In Sec. II, we present the time-domain symbol-rate sampled and oversampled OSDM signal models. Furthermore, in Sec. III, we describe the proposed oversampled OSDM receiver design with an emphasis on Doppler compensation, channel equalization, and estimation methods. The numerical simulations and experimental results are then presented in Sec. IV. Finally, conclusions are drawn in Sec. V.

A. Notation

Bold upper (lower) letters denote matrices (column vectors); $(\cdot)^*$, $(\cdot)^T$, and $(\cdot)^H$ stand for conjugate, transpose, and Hermitian transpose, respectively; $\|\cdot\|$ denotes the Euclidean norm. We define $[\mathbf{x}]_{m:n}$ as the subvector of $\mathbf{x}$ from entry m to n, and $[\mathbf{X}]_{m:n,p:q}$ as the submatrix of $\mathbf{X}$ from row m to n and from column p to q, where only the colon is kept when all rows or columns are included. Moreover, diag$\{\mathbf{x}\}$ is a diagonal matrix created from the vector $\mathbf{x}$; $\mathbf{F}_N$ and $\mathbf{I}_N$ are the $N \times N$ DFT and identity matrix, respectively. Also, $\mathbf{0}_N$ ($\mathbf{1}_N$) denotes the $N \times 1$ all-zero (all-one) vector; $\mathbf{f}_N(n)$ and $\mathbf{i}_N(n)$ are the nth columns of $\mathbf{F}_N$ and $\mathbf{I}_N$, respectively.

II. SIGNAL MODEL

In this section, we present the signal model of the time-domain oversampled OSDM system. For simplicity, we here focus only on time-invariant channels, while deferring the receiver design for time-varying UWA channels to Sec. III.

A. Symbol-rate sampled OSDM

We start by reviewing the baseband signal model of symbol-rate sampled OSDM. Consider a block of $K = MN$ symbols drawn from a unit-energy constellation and denote it by $\mathbf{d} = [d_0, d_1, \ldots, d_{K-1}]^T$. At the transmitter, compared to conventional OFDM modulation where the block is processed by a single K-point IDFT, the OSDM modulation is implemented by performing M component-wise N-point IDFTs, i.e.,

$$\mathbf{s} = (\mathbf{F}_N^H \otimes \mathbf{I}_M)\mathbf{d}, \tag{1}$$

where $\otimes$ denotes the Kronecker product. After that, a cyclic prefix (CP) is added at the beginning of each block to eliminate inter-block interference. Then, the resulting baseband signal is upconverted to the carrier frequency and forwarded to the transmit transducer. It can be easily verified that the OSDM signal model in Eq. (1) is equivalent to that of conventional OFDM and SCBT when $M = 1$ and $M = K$, respectively. As two extreme cases, OFDM has the highest PAPR and lowest diversity, yet enables the most flexible bandwidth and energy management, while SCBT corresponds to the opposite situation. When M increases from 1 to K, OSDM offers multiple PAPR/diversity/flexibility trade-offs to aid system design.

At the receiver, after downconversion and CP removal, the baseband symbol-rate sampled received signal can be expressed as

$$\mathbf{r} = \tilde{\mathbf{C}}\mathbf{s} + \mathbf{n}, \tag{2}$$

where $\tilde{\mathbf{C}}$ is the $K \times K$ circulant channel matrix with the first column equal to the symbol-rate sampled channel impulse response (CIR) vector $\mathbf{c} = [c_0, c_1, \ldots, c_L]^T$ appended by $K - L - 1$ zeros, and $\mathbf{n}$ is the $K \times 1$ noise term. The OSDM demodulation is implemented by performing M component-wise N-point DFTs, i.e.,

$$\mathbf{x} = (\mathbf{F}_N \otimes \mathbf{I}_M)\mathbf{r}, \tag{3}$$

where $\mathbf{x} = [x_0, x_1, \ldots, x_{K-1}]^T$ is the $K \times 1$ demodulated block. In addition, by plugging Eqs. (1) and (2) into Eq. (3), the demodulated block can be rewritten as

$$\mathbf{x} = \mathbf{C}\mathbf{d} + \mathbf{z}, \tag{4}$$

where $\mathbf{C} = (\mathbf{F}_N \otimes \mathbf{I}_M)\tilde{\mathbf{C}}(\mathbf{F}_N^H \otimes \mathbf{I}_M)$ is the $K \times K$ composite channel matrix and $\mathbf{z} = (\mathbf{F}_N \otimes \mathbf{I}_M)\mathbf{n}$ is the $K \times 1$ demodulated noise.

Let us partition the two blocks $\mathbf{d}$ and $\mathbf{x}$ into N vectors of length M, i.e., $\mathbf{d} = [\mathbf{d}_0^T, \mathbf{d}_1^T, \ldots, \mathbf{d}_{N-1}^T]^T$ and $\mathbf{x} = [\mathbf{x}_0^T, \mathbf{x}_1^T, \ldots, \mathbf{x}_{N-1}^T]^T$, where $\mathbf{d}_n = [\mathbf{d}]_{nM:nM+M-1}$ and $\mathbf{x}_n = [\mathbf{x}]_{nM:nM+M-1}$ are referred to as the nth symbol vector and the nth demodulated vector, respectively. It has been proven in Ref. 14 that, over time-invariant channels, the processing of these OSDM vectors can be decoupled. More specifically, in this case the composite channel matrix $\mathbf{C}$ has a block diagonal structure, i.e.,

$$\mathbf{C} = \begin{bmatrix} \mathbf{C}_0 & & & \\ & \mathbf{C}_1 & & \\ & & \ddots & \\ & & & \mathbf{C}_{N-1} \end{bmatrix}, \tag{5}$$

where, for $n = 0, 1, \ldots, N-1$,

$$\mathbf{C}_n = \mathbf{\Lambda}_M^{nH} \mathbf{F}_M^H \mathbf{H}_n \mathbf{F}_M \mathbf{\Lambda}_M^n, \tag{6}$$

$$\mathbf{H}_n = \mathrm{diag}\{\left[H_n, H_{N+n}, \ldots, H_{(M-1)N+n}\right]^T\}, \tag{7}$$

with $\mathbf{\Lambda}_M^n = \mathrm{diag}\{[1, e^{-j2\pi n/K}, \ldots, e^{-j2\pi n(M-1)/K}]^T\}$ and $H_k = \sum_{l=0}^{L} c_l e^{-j(2\pi/K)lk}$ for $k = 0, 1, \ldots, K-1$. Then, from Eqs. (3)–(6), we have

$$\mathbf{x}_n = \left[\mathbf{f}_N^T(n) \otimes \mathbf{I}_M\right]\mathbf{r} = \mathbf{C}_n \mathbf{d}_n + \mathbf{z}_n, \tag{8}$$

where $\mathbf{z}_n = [\mathbf{z}]_{nM:nM+M-1}$ is the nth noise vector. Therefore, analogous to per-subcarrier processing in conventional OFDM, per-vector equalization can be adopted in OSDM.

B. Time-domain oversampled OSDM

We proceed to establish the baseband signal model of time-domain oversampled OSDM over time-invariant channels. In contrast to symbol-rate sampled OSDM, the received signal is now sampled at a rate G/T_s, where T_s is the symbol period and G is the oversampling factor. In this case, the received signal is of length $\underline{K} = GK$ and denoted by $\underline{\mathbf{r}}$. Meanwhile, the CIR vector is of length $\underline{L} = GL$ and denoted by $\underline{\mathbf{c}} = [\underline{c}_0, \underline{c}_1, \ldots, \underline{c}_{\underline{L}}]^T$. Similar to Eq. (2), we can have

$$\underline{\mathbf{r}} = \underline{\tilde{\mathbf{C}}}\,\underline{\mathbf{s}} + \underline{\mathbf{n}}, \tag{9}$$

where $\underline{\tilde{\mathbf{C}}}$ is the $\underline{K} \times \underline{K}$ circulant channel matrix with the first column equal to the oversampled CIR vector $\underline{\mathbf{c}}$ appended by $\underline{K} - \underline{L} - 1$ zeros,

$$\underline{\mathbf{s}} = \mathbf{s} \otimes \mathbf{i}_G(0) = (\mathbf{F}_N^H \otimes \mathbf{I}_{\underline{M}})\underline{\mathbf{d}} \tag{10}$$

is the $\underline{K} \times 1$ transmitted signal with $\underline{\mathbf{d}} = \mathbf{d} \otimes \mathbf{i}_G(0)$ and $\underline{M} = GM$, and $\underline{\mathbf{n}}$ is the $\underline{K} \times 1$ noise term. The OSDM demodulation in this case needs to be reformulated as

$$\underline{\mathbf{x}} = (\mathbf{F}_N \otimes \mathbf{I}_{\underline{M}})\underline{\mathbf{r}} = \underline{\mathbf{C}}\,\underline{\mathbf{d}} + \underline{\mathbf{z}}, \tag{11}$$

where we have defined $\underline{\mathbf{C}} = (\mathbf{F}_N \otimes \mathbf{I}_{\underline{M}})\underline{\tilde{\mathbf{C}}}(\mathbf{F}_N^H \otimes \mathbf{I}_{\underline{M}})$ and $\underline{\mathbf{z}} = (\mathbf{F}_N \otimes \mathbf{I}_{\underline{M}})\underline{\mathbf{n}}$.

Moreover, analogous to the symbol-rate sampled OSDM case, it can be derived that (see Appendix A for a brief proof)

$$\underline{\mathbf{C}} = \begin{bmatrix} \underline{\mathbf{C}}_0 & & & \\ & \underline{\mathbf{C}}_0 & & \\ & & \ddots & \\ & & & \underline{\mathbf{C}}_{N-1} \end{bmatrix}, \tag{12}$$

where, for $n = 0,1,\ldots,N-1$,

$$\underline{\mathbf{C}}_n = \underline{\mathbf{\Lambda}}_{\underline{M}}^{nH} \mathbf{F}_{\underline{M}}^H \underline{\mathbf{H}}_n \mathbf{F}_{\underline{M}} \underline{\mathbf{\Lambda}}_{\underline{M}}^n, \tag{13}$$

$$\underline{\mathbf{H}}_n = \mathrm{diag}\{\left[\underline{H}_n, \underline{H}_{N+n}, \ldots, \underline{H}_{(\underline{M}-1)N+n}\right]^T\}, \tag{14}$$

with $\underline{\mathbf{\Lambda}}_{\underline{M}}^n = \mathrm{diag}\{[1, e^{-j2\pi n/\underline{K}}, \ldots, e^{-j2\pi n(\underline{M}-1)/\underline{K}}]^T\}$ and $\underline{H}_k = \sum_{l=0}^{\underline{L}} \underline{c}_l e^{-j(2\pi/\underline{K})lk}$ for $k = 0, 1, \ldots, \underline{K}-1$. In this case, vector-wise decoupling can still be achieved, since

$$\underline{\mathbf{x}}_n = \left[\mathbf{f}_N^T(n) \otimes \mathbf{I}_{\underline{M}}\right]\underline{\mathbf{r}} = \underline{\mathbf{C}}_n \underline{\mathbf{d}}_n + \underline{\mathbf{z}}_n, \tag{15}$$

where $\underline{\mathbf{d}}_n = [\underline{\mathbf{d}}]_{n\underline{M}:n\underline{M}+\underline{M}-1}$, $\underline{\mathbf{x}}_n = [\underline{\mathbf{x}}]_{n\underline{M}:n\underline{M}+\underline{M}-1}$ and $\underline{\mathbf{z}}_n = [\underline{\mathbf{z}}]_{n\underline{M}:n\underline{M}+\underline{M}-1}$ are the nth oversampled symbol vector, demodulated vector, and noise vector, respectively. It can be seen that Eqs. (11)–(15) are a straightforward extension of Eqs. (3)–(8) in the symbol-rate sampled OSDM case.

As mentioned in Ref. 14, OSDM can be considered as a form of precoded OFDM. Specifically, in symbol-rate sampled OSDM, the nth symbol vector is precoded by $\mathbf{F}_M \mathbf{\Lambda}_M^n$. Intra-vector frequency diversity is thus achieved since each symbol is actually modulated on M subcarriers (which correspond to the channel coefficients $\{H_{mN+n}\}_{m=0}^{M-1}$). As a comparison, in time-domain oversampled OSDM, the energy of each symbol is scattered more widely over $\underline{M}$ subcarriers (which correspond to the channel coefficients $\{\underline{H}_{mN+n}\}_{m=0}^{\underline{M}-1}$), by which a larger frequency diversity gain can be expected.

III. RECEIVER DESIGN OVER UWA CHANNELS

A. Doppler compensation

In Sec. II, the time-invariant channel assumption is key to produce the decoupled per-vector processing in Eqs. (8) and (15). However, in practice UWA channels are typically time-varying, which may destroy orthogonality among symbol vectors and thus lead to IVI.[14] To mitigate the IVI effect, the two-step Doppler compensation method in Ref. 21 is adopted here. It assumes that during one block the time variation on all channel paths can be modeled by a common Doppler scale, under which front-end resampling is first conducted to counteract the wideband Doppler effect. Since the residual Doppler scale is generally much smaller, the post-resampling Doppler distortion can then be considered approximately as a narrowband carrier frequency offset (CFO). Accordingly, in the second step, CFO compensation is further used to make the channel time-invariant.

As for Doppler estimation, in the proposed OSDM receiver the Doppler scaling factor is coarsely estimated by using two linear frequency-modulated (LFM) segments, and the CFO estimate is obtained by minimizing the total IVI energy on some prearranged zero vectors. Specifically, let $\mathcal{S}_z$ be the index set of the zero vectors, i.e., $\mathbf{d}_n = \mathbf{0}_M$ for $n \in \mathcal{S}_z$. Moreover, based on Eq. (15), we define the Doppler compensated vector as $\underline{\mathbf{x}}_n(\epsilon) = [\mathbf{f}_N^T(n) \otimes \mathbf{I}_{\underline{M}}]\underline{\mathbf{\Gamma}}^H(\epsilon)\underline{\mathbf{r}}$, where ϵ is the remaining CFO parameter and $\underline{\mathbf{\Gamma}}(\epsilon) = \mathrm{diag}\{[1, e^{j2\pi\epsilon T_s/G}, \ldots, e^{j2\pi(\underline{K}-1)\epsilon T_s/G}]\}$. Then, the CFO estimate of the time-domain oversampled OSDM system can be obtained as

$$\hat{\epsilon} = \arg\min_{\epsilon} \left\{ \sum_{n \in \mathcal{S}_z} \|\underline{\mathbf{x}}_n(\epsilon)\|^2 \right\}. \tag{16}$$

B. Channel equalization

We here focus on the minimum mean-square error (MMSE) equalization of the time-domain oversampled OSDM system. From Sec. II, it is known that, when the channel can be considered time-invariant after Doppler

compensation, decoupled equalization can be performed on each symbol vector. To gain a better understanding, let us again consider the symbol-rate sampled OSDM case for comparison. Defining $\bar{\mathbf{d}}_n = \mathbf{F}_M \mathbf{\Lambda}_M^n \mathbf{d}_n$, $\bar{\mathbf{x}}_n = \mathbf{F}_M \mathbf{\Lambda}_M^n \mathbf{x}_n$, and $\bar{\mathbf{z}}_n = \mathbf{F}_M \mathbf{\Lambda}_M^n \mathbf{z}_n$, then from Eqs. (6) and (8) we have

$$\bar{\mathbf{x}}_n = \mathbf{H}_n \bar{\mathbf{d}}_n + \bar{\mathbf{z}}_n. \tag{17}$$

Similarly, for the time-domain oversampled OSDM case, we can define $\underline{\bar{\mathbf{d}}}_n = \mathbf{F}_{\underline{M}} \mathbf{\Lambda}_{\underline{M}}^n \underline{\mathbf{d}}_n$, $\underline{\bar{\mathbf{x}}}_n = \mathbf{F}_{\underline{M}} \mathbf{\Lambda}_{\underline{M}}^n \underline{\mathbf{x}}_n$, and $\underline{\bar{\mathbf{z}}}_n = \mathbf{F}_{\underline{M}} \mathbf{\Lambda}_{\underline{M}}^n \underline{\mathbf{z}}_n$. Then, based on Eqs. (13) and (15), we obtain

$$\underline{\bar{\mathbf{x}}}_n = \underline{\mathbf{H}}_n \underline{\bar{\mathbf{d}}}_n + \underline{\bar{\mathbf{z}}}_n. \tag{18}$$

Two remarks on Eq. (18) are in order. First, since $\underline{\mathbf{d}}_n$ is actually an upsampled version of $\mathbf{d}_n$, it can be verified that $\underline{\bar{\mathbf{d}}}_n$ in Eq. (18) has a periodic repetition form

$$\underline{\bar{\mathbf{d}}}_n = \frac{1}{\sqrt{G}} (\mathbf{1}_G \otimes \bar{\mathbf{d}}_n). \tag{19}$$

Then, by defining the $M \times M$ submatrices $\underline{\mathbf{H}}_{n,g} = [\underline{\mathbf{H}}_n]_{gM:gM+M-1,gM:gM+M-1}$, $0 \le g \le G-1$, Eq. (18) can be further rewritten as

$$\underline{\bar{\mathbf{x}}}_n = \frac{1}{\sqrt{G}} \begin{bmatrix} \underline{\mathbf{H}}_{n,0} \\ \underline{\mathbf{H}}_{n,1} \\ \vdots \\ \underline{\mathbf{H}}_{n,G-1} \end{bmatrix} \bar{\mathbf{d}}_n + \underline{\bar{\mathbf{z}}}_n. \tag{20}$$

A comparison between Eqs. (17) and (20) shows that each symbol vector in time-domain oversampled OSDM is equivalently transmitted on G channels corresponding to $\{\underline{\mathbf{H}}_{n,g}\}_{g=0}^{G-1}$, by which more diversity gain can be obtained (apart from the intra-vector frequency diversity in symbol-rate sampled OSDM). However, it should also be noted that, since these virtual channels are typically correlated, the diversity order thus achieved will be less than G.[19] Second, when there exist residual channel time variations after Doppler compensation, the vector $\underline{\bar{\mathbf{z}}}_n$ in Eq. (18) will contain not only the additive noise but also the IVI. To ease the implementation of MMSE equalization, in this paper we assume $\underline{\bar{\mathbf{z}}}_n$ in Eq. (18) (or equivalently $\underline{\mathbf{z}}_n$) is white with zero mean and variance σ^2.

Based on the above remarks and Eq. (20), the MMSE equalization for the time-domain oversampled OSDM system takes the form

$$\hat{\mathbf{d}}_n = \frac{1}{\sqrt{G}} \mathbf{\Lambda}_M^{nH} \mathbf{F}_M^H \mathbf{W}_n \underline{\bar{\mathbf{x}}}_n, \tag{21}$$

where $\hat{\mathbf{d}}_n$ is the estimate of the nth symbol vector, and

$$\mathbf{W}_n = \left(\frac{1}{G} \sum_{g=0}^{G-1} \underline{\mathbf{H}}_{n,g}^H \underline{\mathbf{H}}_{n,g} + \sigma^2 \mathbf{I}_M \right)^{-1} \left[\underline{\mathbf{H}}_{n,0}^H, \underline{\mathbf{H}}_{n,1}^H, \ldots, \underline{\mathbf{H}}_{n,G-1}^H \right] \tag{22}$$

is the corresponding $M \times \underline{M}$ coefficient matrix of the MMSE equalizer. It can be seen that, when $G = 1$, the channel equalization in Eqs. (21) and (22) reduces to that of symbol-sampled OSDM in Ref. 14. Moreover, it is interesting to note that, since the submatrices $\{\underline{\mathbf{H}}_{n,g}\}$ are all diagonal, the complexity of the MMSE equalization in Eq. (21) is approximately linear in M per vector.

C. Channel estimation

In practice, the computation of the weight matrix $\mathbf{W}_n$ in Eq. (22) necessitates estimation of the oversampled CIR vector $\underline{\mathbf{c}}$ and the noise variance σ^2.

To this end, a pilot-assisted method similar to that in Ref. 22 is adopted to estimate $\underline{\mathbf{c}}$. Specifically, we use U equi-spaced pilot vectors in each block and assume that $U\underline{M} > \underline{L}$. Let $\mathcal{S}_p = \{p_0, p_1, \ldots, p_{U-1}\}$ be the index set of the pilot vectors, where $p_u = u\Delta$ for $u = 0, 1, \ldots, U-1$ with $\Delta = N/U$ being an integer. From Eqs. (14), (18), and (19), it can be obtained that

$$\underline{\bar{\mathbf{x}}}_p = \mathbf{\Pi}_p \underline{\mathbf{c}} + \underline{\bar{\mathbf{z}}}_p, \quad p \in \mathcal{S}_p, \tag{23}$$

where

$$\mathbf{\Pi}_p = \frac{1}{\sqrt{G}} (\mathbf{I}_G \otimes \bar{\mathbf{D}}_p) \tilde{\mathbf{F}}_{\underline{M}} \mathbf{\Lambda}_{\underline{L}+1}^p, \tag{24}$$

with $\bar{\mathbf{D}}_p = \mathrm{diag}\{\bar{\mathbf{d}}_p\}$ and $\tilde{\mathbf{F}}_{\underline{M}} = [\mathbf{1}_U^T \otimes \sqrt{\underline{M}} \mathbf{F}_{\underline{M}}]_{:,0:\underline{L}}$.

Then, by stacking the U pilot vectors together, and defining $\underline{\bar{\mathbf{x}}}_{\mathcal{P}} = [\underline{\bar{\mathbf{x}}}_{p_0}^T, \underline{\bar{\mathbf{x}}}_{p_1}^T, \ldots, \underline{\bar{\mathbf{x}}}_{p_{U-1}}^T]^T$ and $\mathbf{\Pi}_{\mathcal{P}} = [\mathbf{\Pi}_{p_0}^T, \mathbf{\Pi}_{p_1}^T, \ldots, \mathbf{\Pi}_{p_{U-1}}^T]^T$, we can obtain the least-squares estimate of the oversampled CIR vector

$$\hat{\underline{\mathbf{c}}} = (\mathbf{\Pi}_{\mathcal{P}}^H \mathbf{\Pi}_{\mathcal{P}})^{-1} \mathbf{\Pi}_{\mathcal{P}}^H \underline{\bar{\mathbf{x}}}_{\mathcal{P}}. \tag{25}$$

Moreover, to further ease the computation, we follow the same strategy as in Ref. 22 and select U frequency-shifted Chu sequences to be the pilot vectors, i.e.,

$$\mathbf{d}_p = \mathbf{\Lambda}_M^{pH} \mathbf{b}_M, \quad p \in \mathcal{S}_p, \tag{26}$$

with $\mathbf{b}_M$ being a Chu sequence of length M. In this case, we can avoid matrix inversion since $\mathbf{\Pi}_{\mathcal{P}}^H \mathbf{\Pi}_{\mathcal{P}} = MU\mathbf{I}_{\underline{L}+1}$ (see Appendix B), and thus simplify the channel estimation as

$$\hat{\underline{\mathbf{c}}} = \frac{1}{\sqrt{G}MU} \sum_{p \in \mathcal{S}_p} \mathbf{\Lambda}_{\underline{L}+1}^{pH} \tilde{\mathbf{F}}_{\underline{M}}^H \left(\mathbf{I}_G \otimes \bar{\mathbf{D}}_p^H \right) \underline{\bar{\mathbf{x}}}_p. \tag{27}$$

On the other hand, to estimate σ^2, we resort again to the zero vectors in the OSDM block. The noise variance can be measured as the average power of their corresponding demodulated vectors after Doppler compensation. Mathematically, we have the estimate

$$\hat{\sigma}^2 = \frac{1}{GMV} \sum_{\mathrm{n} \in \mathcal{S}_z} \| \mathbf{x}_n(\hat{\epsilon}) \|^2, \tag{28}$$

where V is the cardinality of $\mathcal{S}_z$, i.e., the number of zero vectors in each block.

IV. SIMULATION AND EXPERIMENTAL RESULTS

A. Numerical simulation results

We first evaluate the bit error rate (BER) performance of the proposed time-domain oversampled OSDM system by

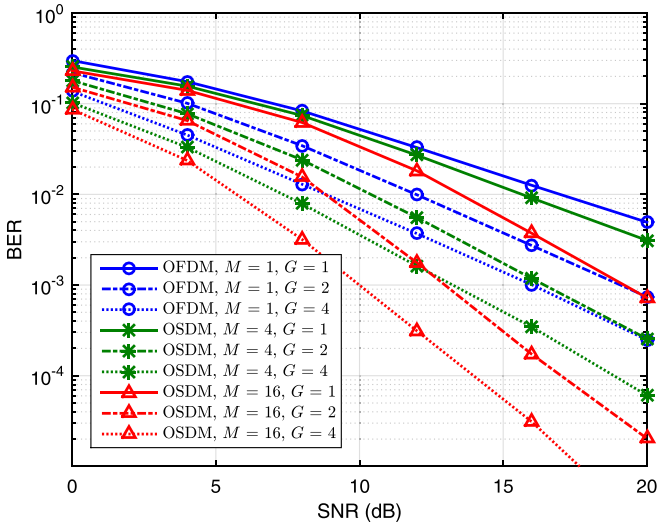

FIG. 1. (Color online) BER performance of the proposed time-domain oversampled OSDM system with known CIR vector $\underline{\mathbf{c}}$ and no Doppler effect ($a=0$).

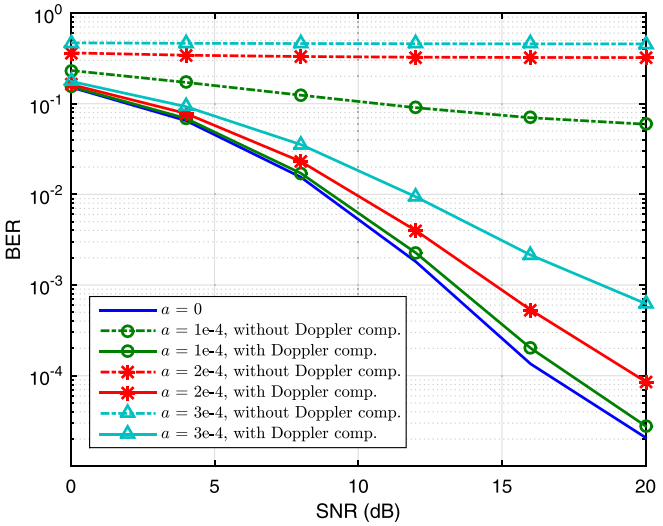

FIG. 2. (Color online) BER performance of the proposed time-domain oversampled OSDM system with known CIR vector $\underline{\mathbf{c}}$ and different Doppler scaling factors.

means of numerical simulations. Here, each OSDM block contains $K=1024$ quaternary phase-shift keying symbols. We set the interval of each symbol to $T_s=0.25$ ms, yielding a data rate of 8 kbit/s, and the block duration is $T=KT_s=256$ ms. Moreover, a CP of length $K_g=128$ and a carrier frequency of $f_c=6$ kHz are used.

In addition, the simulated UWA channel consists of six discrete paths and has a uniform power delay profile. The path amplitudes are assumed to be complex Gaussian distributed, giving rise to Rayleigh fading, while the path delays are randomly distributed with maximum delay spread equal to $\tau_{\max}=78T_s=19.5$ ms. Moreover, the pulse-shaping filter is set to be a truncated raised cosine pulse of support $2T_s$ with a roll-off factor $\beta=0.5$. Therefore, it can be obtained that the overall bandwidth is about $(1+\beta)/T_s=6$ kHz, and the overall channel memory spans $L=80$ symbols, which corresponds to a total channel delay spread of $LT_s=20$ ms. On the other hand, the channel time variation here is simulated by a post-resampling Doppler scaling factor a. Since the UWA communication signal is typically wideband (which is the case in these simulations), we take the nonuniform Doppler shift effect into account explicitly. Specifically, by treating OSDM as a version of precoded OFDM, the Doppler shift imposed on the kth subcarrier is af_k, where f_k is the subcarrier frequency.

Figure 1 shows the BER performance of the proposed time-domain oversampled OSDM system over time-invariant channels with perfect channel knowledge. We here consider three vector lengths $M=1$, 4, 16 and three oversampling factors $G=1$, 2, 4. As mentioned in Sec. II, OSDM is actually equivalent to OFDM when $M=1$. Moreover, the time-domain oversampled system reduces to the standard symbol-rate sampled one when $G=1$. The BER curves of these systems are included to serve as benchmarks. Against them, it can be seen that, when G is fixed, the system performance improves as M increases. This is because a longer vector length has the potential to provide more intra-vector frequency diversity gain.[15] On the other hand, as explained in Eq. (20), a larger oversampling factor G can also contribute to the intra-vector frequency diversity gain. As such, when M is fixed, a better system performance can be obtained by increasing G. However, it should be noted that, since the virtual channels produced by time-domain oversampling are correlated, the diversity order thus obtained will not increase linearly with G. As a proof, it can be seen in Fig. 1 that the slope of the BER performance curves almost keeps constant when G increases from 2 to 4. A similar observation was also made in Ref. 19 for the OFDM case. Therefore, in practice there is always a trade-off between the diversity gain and the computational complexity induced by time-domain oversampling.

We evaluate the impact of the channel Doppler effect on the proposed time-domain oversampled OSDM system in Fig. 2. In this case, the vector length is set to $M=16$ and the oversampling factor is fixed to $G=2$. In addition, similar to

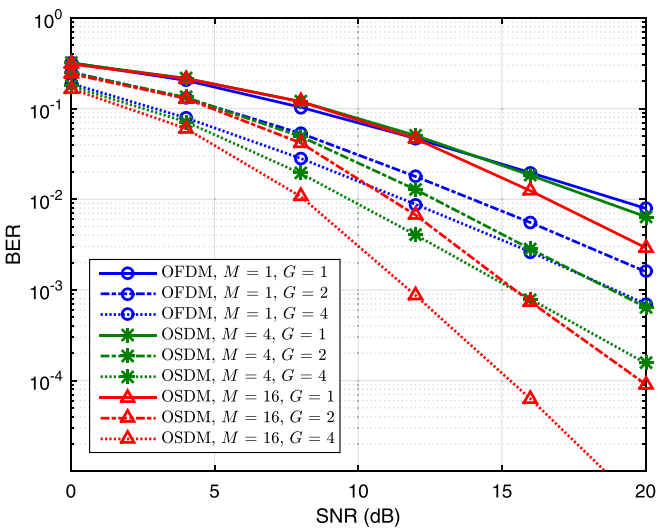

FIG. 3. (Color online) BER performance of the proposed time-domain oversampled OSDM system with estimated CIR vector $\hat{\underline{\mathbf{c}}}$ and no Doppler effect ($a=0$).

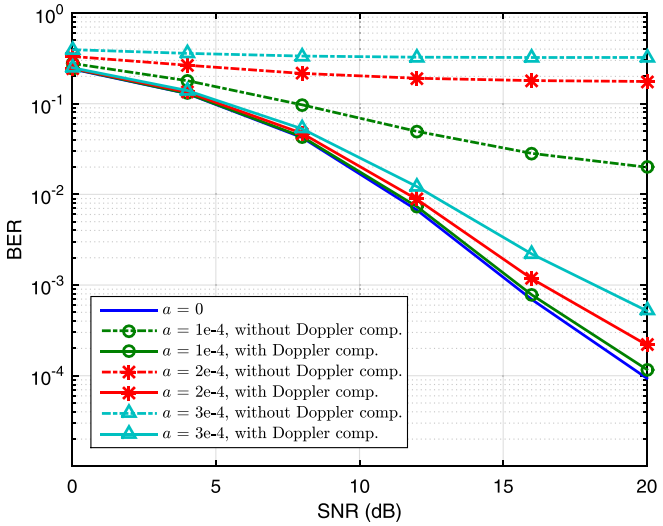

FIG. 4. (Color online) BER performance of the proposed time-domain oversampled OSDM system with estimated CIR vector $\hat{\underline{\mathbf{c}}}$ and different Doppler scaling factors.

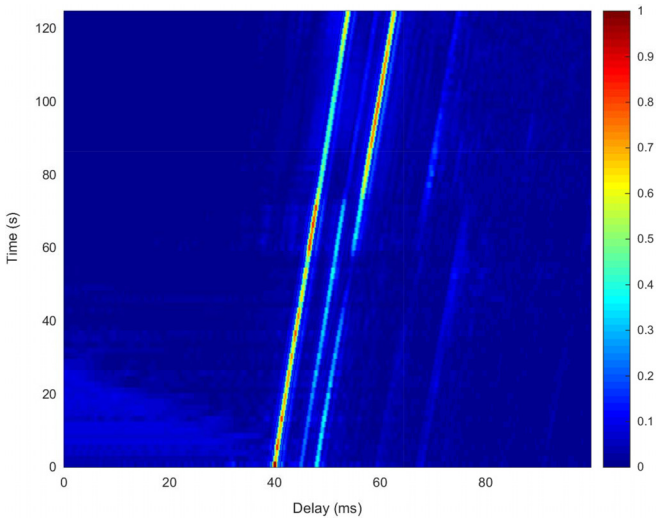

FIG. 6. (Color online) Magnitude of the time-varying CIR measured during 80 data frames.

Fig. 1, it is assumed that the CIR vector $\underline{\mathbf{c}}$ is known *a priori*. The channel Doppler effect is introduced here by setting different Doppler scaling factors $a = 1 \times 10^{-4}$, 2×10^{-4}, and 3×10^{-4}. Moreover, to benchmark the system performance, the time-invariant case (i.e., $a = 0$) is also included. We now compare the BERs of the proposed oversampled OSDM system with and without Doppler compensation. It can be seen that, in the absence of Doppler compensation, the OSDM system almost fails to function due to the excessive IVI at $a = 2 \times 10^{-4}$ and 3×10^{-4}. In contrast, by using the zero-vector-based method of Sec. III A, the OSDM system performance can be significantly improved. However, since the post-resampling Doppler distortion is actually wideband here, it cannot be perfectly canceled by a narrowband CFO compensation. Therefore, as a increases, the residual Doppler effect gets nonnegligible, and the OSDM system performance degrades accordingly.

Next, we take the channel estimation error into account in Figs. 3 and 4. Here, the simulation configurations are the same as those in Figs. 1 and 2. The only difference is that a total of $UM = 128$ pilot symbols are used, by which we have $UM > L$ (or equivalently $U\underline{M} > \underline{L}$), and thus the CIR vector estimate $\hat{\underline{\mathbf{c}}}$ can be computed as in Eq. (27). It is not surprising that here we have similar observations as those in Figs. 1 and 2, except that the BER curve rises slightly in most cases due to the channel estimation error.

B. Experimental results

A field experiment was also conducted to test the performance of the proposed time-domain oversampled OSDM system at the Danjiangkou reservoir, Henan Province, China, in June 2017. The water depth at the experiment site was about 40–50 m. The transducer was suspended at 25 m from a surface ship, while a single-element hydrophone was submerged at a depth of 27 m from an anchored ship. The transceiver separation was about 150 m. During the experiment, there were a total of 80 data frames transmitted consecutively, each of which had the structure shown in Fig. 5. It contained three uncoded OSDM blocks with $M = 1$ (i.e., OFDM), 4, and 16. The parameter setup of these blocks was nearly the same as that used in Sec. IV A. The only difference is that the CP length was extended to $K_g = 256$ in the experiment to accommodate a longer channel delay spread $K_g T_s = 64$ ms, and therefore the entire OSDM block duration was $(K_g + K)T_s = 320$ ms. In addition, two tone segments were inserted to identify the frame, and a leading LFM segment was added to perform synchronization. Moreover, the LFM segments of two neighboring frames were also used to estimate the Doppler scaling factor. All these auxiliary signal segments had a duration of 200 ms.

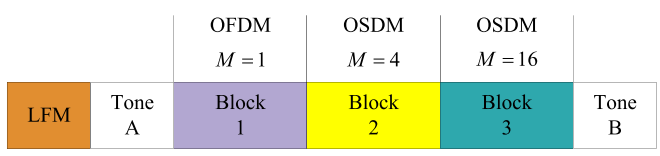

FIG. 5. (Color online) Frame structure used in the field experiment.

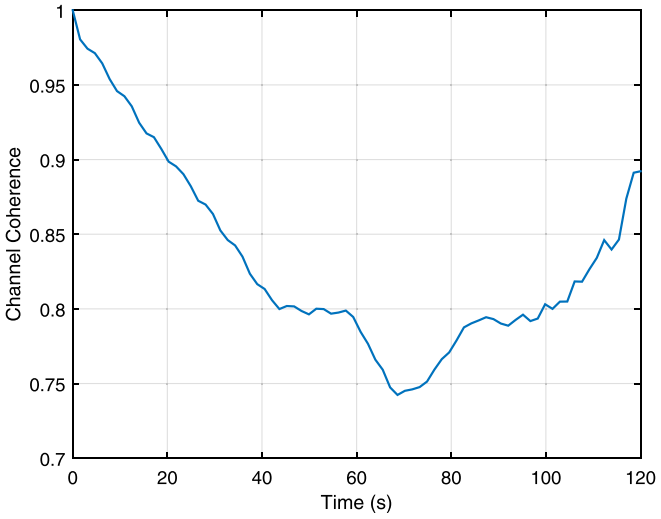

FIG. 7. (Color online) Interframe temporal coherence of the experimental channel.

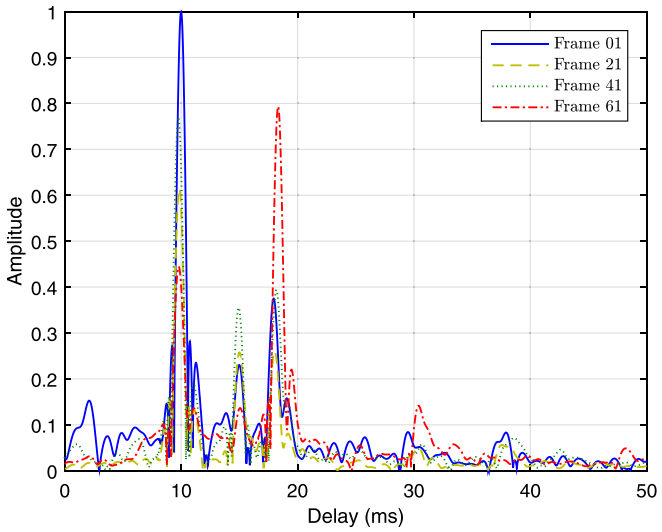

FIG. 8. (Color online) Snapshots of the measured CIR magnitude at frames 01, 21, 41, and 61.

Figure 6 displays the magnitude of the time-varying CIR measured by correlation with the LFM segments in 80 data frames. Furthermore, to achieve a better understanding of the experimental channel, Fig. 7 shows its interframe temporal coherence, and Fig. 8 presents the CIR snapshots at frames 01, 21, 41, and 61. It can be seen that the channel is relatively benign and features a sparse multipath structure; however, there exist obvious path amplitude fluctuations and the strongest path changes with time. The maximum delay spread of the channel was about $\tau_{\max} = 40$ ms. Meanwhile, although no intentional platform motion was involved, the nonstationary current and the mismatch between the transceiver oscillators caused approximately a constant Doppler scale. This effect is indicated by the slope of the lines in Fig. 6. Specifically, within the observation duration of 80 data frames, i.e., a total of 124.8 s, the channel multipath structure was lagged by 14.25 ms, which corresponds to an average Doppler scaling factor of $\bar{a} = -1.14 \times 10^{-4}$.

The Doppler scaling factor and residual CFO estimates produced by the two-step Doppler compensation method are

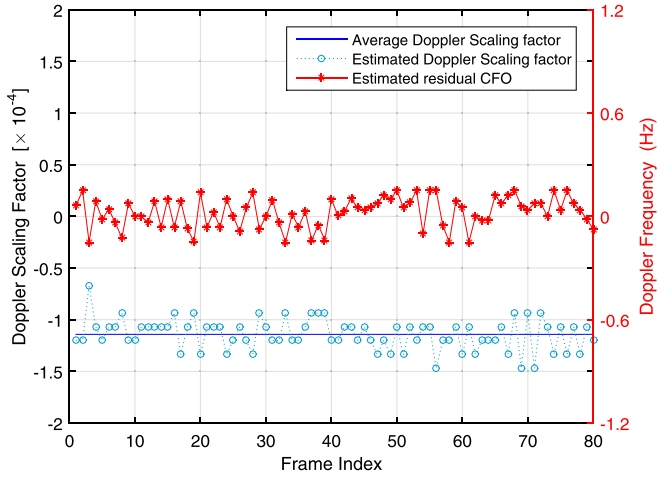

FIG. 9. (Color online) Estimated Doppler scaling factor and residual CFO at each frame.

TABLE I. Output SNR performance of the proposed time-domain oversampled OSDM system in the experiment.

	OFDM	OSDM	
	$M=1$	$M=4$	$M=16$
$G=1$	2.26 dB	4.56 dB	5.46 dB
$G=2$	2.50 dB	4.80 dB	5.70 dB
$G=4$	2.58 dB	4.93 dB	5.81 dB

shown in Fig. 9. It can be seen that the Doppler scaling factor estimate is centered at the average Doppler scaling factor $\bar{a}$ obtained in Fig. 6. By performing the front-end resampling operation, the channel Doppler effect can be significantly reduced, with the residual CFO shifted around zero and confined to a small frequency range [–0.3,0.3] Hz. Then, after channel estimation and equalization, the output signal-to-noise ratio (SNR) and BER of the proposed time-domain oversampled OSDM system are summarized in Tables I and II, respectively. Here, the output SNR is computed as

$$\mathrm{SNR}_{\mathrm{out}} = -10\log\left(\frac{1}{BDM}\sum_{b=1}^{B}\sum_{n\in\mathcal{S}_d}\left\|\mathbf{d}_n^{(b)} - \hat{\mathbf{d}}_n^{(b)}\right\|^2\right), \tag{29}$$

where B is the number of OSDM blocks transmitted in the experiment; D is the number of payload data vectors in each block and $\mathcal{S}_d$ denotes the corresponding vector index set; $\mathbf{d}_n^{(b)}$ and $\hat{\mathbf{d}}_n^{(b)}$ are the nth symbol vector of the bth block and its estimate, respectively.

Similar to the numerical simulation results, the experimental data analysis shows that the system performance improves as M or G increases, which confirms the effectiveness of the proposed OSDM system over practical UWA channels. Figure 10 further plots as an example the BER of the proposed OSDM system with $M = 16$ and the estimated noise variance at each frame. Again, it can be observed that the time-domain oversampled system (with $G = 2$ and 4) outperforms its symbol-rate sampled counterpart (with $G = 1$) at most frames. Moreover, the correlation between the BER performance and the noise variance in Fig. 10, together with the relatively low SNR in Table I, suggests that the complicated channel noise effect may be the main reason for no error-free transmissions achieved in the field experiment.

V. CONCLUSION

In this paper, a time-domain oversampled OSDM system has been designed to establish reliable communication

TABLE II. BER performance of the proposed time-domain oversampled OSDM system in the experiment.

	OFDM	OSDM	
	$M=1$	$M=4$	$M=16$
$G=1$	9.91×10^{-2}	8.05×10^{-2}	5.69×10^{-2}
$G=2$	9.11×10^{-2}	6.89×10^{-2}	4.86×10^{-2}
$G=4$	8.78×10^{-2}	5.80×10^{-2}	4.30×10^{-2}

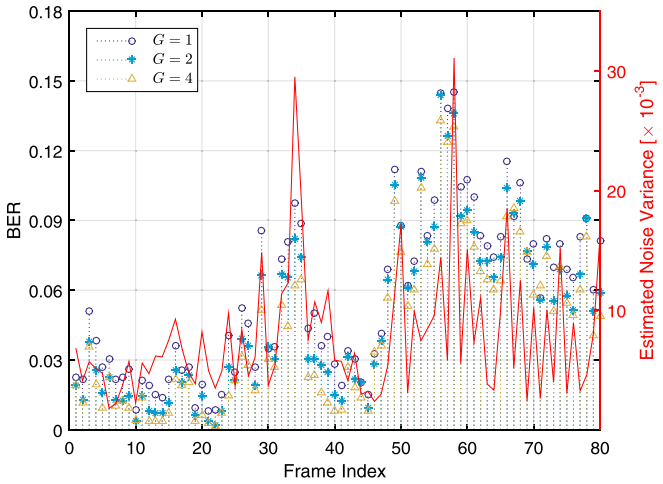

FIG. 10. (Color online) BER of the proposed OSDM system with $M = 16$ and estimated noise variance at each frame.

links over time-varying UWA channels. Similar to standard symbol-rate sampled OSDM, the proposed OSDM system can decouple its vectors at the receiver over frequency-selective fading channels [Eq. (15)]. At the same time, the proposed OSDM system has the capability to combine the diversity gains obtained by precoding (OFDM) and time-domain oversampling, which yields an enhanced intra-vector frequency diversity compared to standard symbol-rate sampled OSDM. In this case, each symbol vector is equivalently transmitted over multiple virtual channels [Eq. (20)], and accordingly at the receiver the per-vector equalization has a similar structure as that used for multi-element reception [Eqs. (21) and (22)]. Although difficult to give any theoretical analysis on the overall intra-vector diversity gain, both the numerical simulations and experimental results have demonstrated the improved system performance thus caused. Moreover, by exploiting the composite channel matrix factorization, the per-vector equalization algorithm approximately has a linear complexity, which makes the proposed time-domain oversampled OSDM system attractive for practical use.

ACKNOWLEDGMENTS

This work was supported by the National Natural Science Foundation of China under Grant Nos. 61771394, 61801394, and 61531015, the Natural Science Basic Research Plan in Shaanxi Province of China under Grant No. 2018JM6042, the Fundamental Research Funds for the Central Universities under Grant No. 3102017JG05007, and the 111 Project under Grant No. B18041. The authors would like to thank all the participants of the field experiment. They would also like to thank Professor Fengzhong Qu for his help on plotting the channel coherence in Fig. 7.

APPENDIX A: PROOF OF COMPOSITE CHANNEL MATRIX STRUCTURE IN EQS. (12)–(14)

The proof is similar to that in Appendix A of Ref. 14. We first perform the DFT matrix factorization

$$\mathbf{F}_{\underline{K}} = \mathbf{P}_{N,\underline{M}}(\mathbf{I}_N \otimes \mathbf{F}_{\underline{M}})\underline{\mathbf{\Lambda}}(\mathbf{F}_N \otimes \mathbf{I}_{\underline{M}}), \tag{A1}$$

where

$$\mathbf{P}_{N,\underline{M}} = \begin{bmatrix} \mathbf{I}_N \otimes \mathbf{i}_{\underline{M}}^T(0) \\ \mathbf{I}_N \otimes \mathbf{i}_{\underline{M}}^T(1) \\ \vdots \\ \mathbf{I}_N \otimes \mathbf{i}_{\underline{M}}^T(\underline{M}-1) \end{bmatrix}, \tag{A2}$$

and

$$\underline{\mathbf{\Lambda}} = \begin{bmatrix} \underline{\mathbf{\Lambda}}_{\underline{M}}^0 & & & \\ & \underline{\mathbf{\Lambda}}_{\underline{M}}^1 & & \\ & & \ddots & \\ & & & \underline{\mathbf{\Lambda}}_{\underline{M}}^{N-1} \end{bmatrix}. \tag{A3}$$

Meanwhile, it is well-known that the circulant channel matrix can be factorized as $\underline{\tilde{\mathbf{C}}} = \mathbf{F}_{\underline{K}}^H \underline{\tilde{\mathbf{H}}} \mathbf{F}_{\underline{K}}$, where $\underline{\tilde{\mathbf{H}}} = \mathrm{diag}\{[\underline{H}_0, \underline{H}_1, \ldots, \underline{H}_{\underline{K}-1}]^T\}$. Moreover, by defining

$$\underline{\mathbf{H}} = \begin{bmatrix} \mathbf{H}_0 & & & \\ & \mathbf{H}_1 & & \\ & & \ddots & \\ & & & \mathbf{H}_{N-1} \end{bmatrix}, \tag{A4}$$

it can be seen that $\underline{\tilde{\mathbf{H}}} = \mathbf{P}_{N,\underline{M}} \underline{\mathbf{H}} \mathbf{P}_{N,\underline{M}}^H$. Based on these matrix factorizations, the composite channel matrix can be rewritten as

$$\begin{aligned} \underline{\mathbf{C}} &= (\mathbf{F}_N \otimes \mathbf{I}_{\underline{M}})\underline{\tilde{\mathbf{C}}}(\mathbf{F}_N^H \otimes \mathbf{I}_{\underline{M}}) \\ &= (\mathbf{F}_N \otimes \mathbf{I}_{\underline{M}})\mathbf{F}_{\underline{K}}^H \mathbf{P}_{N,\underline{M}} \underline{\mathbf{H}} \mathbf{P}_{N,\underline{M}}^H \mathbf{F}_{\underline{K}} (\mathbf{F}_N^H \otimes \mathbf{I}_{\underline{M}}) \\ &= \underline{\mathbf{\Lambda}}^H (\mathbf{I}_N \otimes \mathbf{F}_{\underline{M}}^H) \underline{\mathbf{H}} (\mathbf{I}_N \otimes \mathbf{F}_{\underline{M}}) \underline{\mathbf{\Lambda}}, \end{aligned} \tag{A5}$$

where in the third equality we have used Eq. (A1). Then from Eq. (A5), we can readily obtain Eqs. (12)–(14).

APPENDIX B: PROOF OF ORTHOGONALITY AMONG COLUMNS IN $\mathbf{\Pi}_{\mathcal{P}}$

Since the pilot vectors are equi-spaced with $p_u = u\Delta$, it can be obtained that

$$\mathbf{\Pi}_{\mathcal{P}} = \sqrt{MU}\bar{\mathbf{D}}_{\mathcal{P}} \mathbf{P}_{\underline{M},U} \left[\mathbf{F}_{\underline{M}U}\right]_{:,0:\underline{L}}, \tag{B1}$$

where

$$\bar{\mathbf{D}}_{\mathcal{P}} = \begin{bmatrix} \mathbf{I}_G \otimes \bar{\mathbf{D}}_{p_0} & & & \\ & \mathbf{I}_G \otimes \bar{\mathbf{D}}_{p_1} & & \\ & & \ddots & \\ & & & \mathbf{I}_G \otimes \bar{\mathbf{D}}_{p_{U-1}} \end{bmatrix}. \tag{B2}$$

Moreover, since the frequency-shifted Chu sequences in Eq. (26) are used as pilot vectors, each entry in $\bar{\mathbf{d}}_p$ is actually unit-amplitude, and thus we have $\bar{\mathbf{D}}_{\mathcal{P}}^H \bar{\mathbf{D}}_{\mathcal{P}} = \mathbf{I}_{\underline{M}U}$. Finally, given that $\mathbf{P}_{\underline{M},U}$ and $\mathbf{F}_{\underline{M}U}$ are unitary matrices, we can obtain that $\mathbf{\Pi}_{\mathcal{P}}^H \mathbf{\Pi}_{\mathcal{P}} = MU\mathbf{I}_{\underline{L}+1}$.

[1]M. Stojanovic and J. Preisig, "Underwater acoustic communication channels: Propagation models and statistical characterization," IEEE Commun. Mag. **47**(1), 84–89 (2009).
[2]M. Stojanovic, "Recent advances in high-speed underwater acoustic communications," IEEE J. Ocean. Eng. **21**(2), 125–136 (1996).
[3]D. Kilfoyle and A. Baggeroer, "The state of the art in underwater acoustic telemetry," IEEE J. Ocean. Eng. **25**(1), 4–27 (2000).
[4]S. Zhou and Z. Wang, *OFDM for Underwater Acoustic Communications* (Wiley, Hoboken, NJ, 2014).
[5]M. Stojanovic, J. Catipovic, and J. G. Proakis, "Adaptive multichannel combining and equalization for underwater acoustic communications," J. Acoust. Soc. Am. **94**(3), 1621–1631 (1993).
[6]M. Stojanovic, J. Catipovic, and J. Proakis, "Phase-coherent digital communications for underwater acoustic channels," IEEE J. Ocean. Eng. **19**(1), 100–111 (1994).
[7]M. Stojanovic, J. A. Catipovic, and J. G. Proakis, "Reduced-complexity spatial and temporal processing of underwater acoustic communication signals," J. Acoust. Soc. Am. **98**(2), 961–972 (1995).
[8]Z. Wang and G. B. Giannakis, "Wireless multicarrier communications: Where Fourier meets Shannon," IEEE Signal Process. Mag. **17**(3), 29–48 (2000).
[9]S. H. Han and J. H. Lee, "An overview of peak-to-average power ratio reduction techniques for multicarrier transmission," IEEE Wireless Commun. Mag. **12**(2), 56–65 (2005).
[10]Y. Rahmatallah and S. Mohan, "Peak-to-average power ratio reduction in OFDM systems: A survey and taxonomy," IEEE Commun. Surv. Tutorials **15**(4), 1567–1592 (2013).
[11]N. Suehiro, C. Han, T. Imoto, and N. Kuroyanagi, "An information transmission method using Kronecker product," in *Proc. IASTED Int. Conf. Commun. Syst. Netw.* (2002), pp. 206–209.
[12]N. Suehiro, C. Han, and T. Imoto, "Very efficient wireless frequency usage based on pseudo-coherent addition of multipath signals using Kronecker product with rows of DFT matrix," in *Proc. Int. Symp. Inf. Theory* (2003), pp. 385–385.
[13]X.-G. Xia, "Precoded and vector OFDM robust to channel spectral nulls and with reduced cyclic prefix length in single transmit antenna systems," IEEE Trans. Commun. **49**(8), 1363–1374 (2001).
[14]J. Han, S. P. Chepuri, Q. Zhang, and G. Leus, "Iterative per-vector equalization for orthogonal signal-division multiplexing over time-varying underwater acoustic channels," IEEE J. Ocean. Eng. **44**(1), 240–255 (2019).
[15]Y. Li, I. Ngebani, X.-G. Xia, and A. Host-Madsen, "On performance of vector OFDM with linear receivers," IEEE Trans. Signal Process. **60**(10), 5268–5280 (2012).
[16]T. Ebihara and K. Mizutani, "Underwater acoustic communication with an orthogonal signal division multiplexing scheme in doubly spread channels," IEEE J. Ocean. Eng. **39**(1), 47–58 (2014).
[17]T. Ebihara and G. Leus, "Doppler-resilient orthogonal signal-division multiplexing for underwater acoustic communication," IEEE J. Ocean. Eng. **41**(2), 408–427 (2016).
[18]J. Han, W. Shi, and G. Leus, "Space-frequency coded orthogonal signal-division multiplexing over underwater acoustic channels," J. Acoust. Soc. Am. **141**(6), EL513–EL518 (2017).
[19]C. Tepedelenlioglu and R. Challagulla, "Low-complexity multipath diversity through fractional sampling in OFDM," IEEE Trans. Signal Process. **52**(11), 3104–3116 (2004).
[20]B. Peng, P. S. Rossi, H. Dong, and K. Kansanen, "Time-domain oversampled OFDM communication in doubly-selective underwater acoustic channels," IEEE Commun. Lett. **19**(6), 1081–1084 (2015).
[21]B. Li, S. Zhou, M. Stojanovic, L. Freitag, and P. Willett, "Multicarrier communication over underwater acoustic channels with nonuniform Doppler shifts," IEEE J. Ocean. Eng. **33**(2), 198–209 (2008).
[22]J. Han, L. Zhang, Q. Zhang, and G. Leus, "Low-complexity equalization of orthogonal signal-division multiplexing in doubly-selective channels," IEEE Trans. Signal Process. **67**(4), 915–929 (2019).